Acta Mechanica Sinica (2014) 30(1):73–83
DOI 10.1007/s10409-014-0002-4

RESEARCH PAPER

A continuous-discontinuous cellular automaton method for cracks growth and coalescence in brittle material

Fei Yan · Xia-Ting Feng · Peng-Zhi Pan · Shao-Jun Li

Received: 18 July 2013 / Revised: 10 October 2013 / Accepted: 28 November 2013

Abstract A method of continuous-discontinuous cellular automaton for modeling the growth and coalescence of multiple cracks in brittle material is presented. The method uses the level set to track arbitrary discontinuities, and calculation grids are independent of the discontinuities and no remeshing are required with the crack growing. Based on Griffith fracture theory and Mohr–Coulumb criterion, a mixed fracture criterion for multiple cracks growth in brittle material is proposed. The method treats the junction and coalescence of multiple cracks, and junction criterion and coalescence criterion for brittle material are given, too. Besides, in order to overcome the tracking error in the level set approximation for crack junction and coalescence, a dichotomy searching algorithm is proposed. Introduced the above theories into continuous-discontinuous cellular automaton, the present method can be applied to solving multiple crack growth in brittle material, and only cell stiffness is needed and no assembled global stiffness is needed. Some numerical examples are given to shown that the present method is efficient and accurate for crack junction, coalescence and percolation problems.

The project was supported by the National Key Basic Research Program of China (2013CB036405), the National Natural Science Foundation of China (11002154, 41272349, and 41372315), and the CAS/SAFEA International Partnership Program for Creative Research Teams (KZCX2-YW-T12).

F. Yan (✉) · X.-T. Feng · P.-Z. Pan · S.-J. Li
State Key Laboratory of Geomechanics and Geotechnical Engineering,
Institute of Rock and Soil Mechanics,
Chinese Academy of Science,
430071 Wuhan, China
e-mail: fyan@whrsm.ac.cn

Keywords Continuous-discontinuous cellular automaton method · Multiple crack growth · Discontinuous cellular automaton · Junction criterion · Coalescence criterion

1 Introduction

The presence of crack is a common cause of the failure of structure. Brittle materials such as concrete, ceramics, rock, etc. often contain a large number of flaws and micro-cracks, and the failure for brittle material may occur from the micro-crack growth. With the external loading, micro-crack growth arises, and intersection, coalescence may take place in the process of multiple micro-crack growth. The prediction of crack behavior has always been a challenge for researchers, and crack propagation represents a real concern of engineers designing general structures. So it is important to study multiple crack growth, especially for the process from multiple micro-crack initially propagation, further crack intersection and coalescence, and finally the occurrence of failure.

The mechanics of two interacting cracks in brittle material has been firstly studied in the experiment by Tanaka et al. [1], in which Tanaka studied propagation and closure of small cracks in SiC particulate reinforced aluminum alloy in high cycle and low cycle fatigue. Later Lawler [2] studied hybrid fiber-reinforcement in mortar and concrete, and revealed that the fracture process occurs in three stages: micro-crack formation, micro-crack coalescence and finally the formation of macro-crack. And Barpi and Valente [3] have been studied the size-effects bifurcation phenomena during multiple cohesive crack propagation via experiments.

Analytic solutions for materials containing random distributions of cracks, such as Poisson distributions, were reported by Datsyshin and Savruk [4]. Based on the superposition technique and the idea of self-consistency applied to the average tractions on individual cracks, Kachanov [5, 6] proposed a simple analytic method of stress analysis in elastic solids with many cracks. Later, Rubinstein [7, 8] gave a close form of solution in terms of complex stress potentials

and the exact solution of the interaction of a macro-crack with a single micro-crack, and studied the interaction by different micro-crack spacing. Besides, based on the concept of approximating the crack-generated stress field, a dislocation approximation for calculating crack interaction was introduced by Freij-Ayoub et al. [9].

It is not absolute for all cases to use analytical method to solve multiple crack problems, especially for many cracks and complex location relation of cracks. So it is significant work to develop numerical method to solve multiple crack problems. Chen et al. [10] developed singular integral equations method for random and regular distributions of multiple cracks in an infinite plate. Stochastic methods for the reliability analysis against fatigue failure and the emphasis on the reliability in the presence of sets of cracks were developed by Bolotin [11], furthermore, based on the lognormal random process model and a second order approximation, a simple stochastic crack growth analysis method was proposed for practical application by Yang [12], additionally, Lua and Liu et al. [13, 14] proposed a stochastic damage model for the rupture prediction of a multi-phase solid, in which the stochastic damage model was utilized to quantitatively analyze the effects of uncertainties in locations, orientations and numbers of micro-cracks at the macro-tip. And McDowell [15] adopted the viewpoint that multiple, microstructure interactions and closure effects may simultaneously influence the propagation of small cracks.

Later, fractal methods for multiple cracks problems were studied by Rybaczuk and Stoppel [16], and Lua [17] developed a mixed boundary integral equation method for the analysis of elastic interactions of a fatigue crack with a micro-defect, and further Carpinteri [18] used boundary element method to take the snap-back analysis of fracture evolution in multi-cracked solids. Then Ma et al. [19] combined the concept of the eigen crack opening displacement with boundary integral equations to get an efficient solution of multiple cracks problems. In addition, Budyn et al. [20] described a method for modeling the evolution of multiple cracks in the framework of the extended finite element method, which is a numerical method for treating arbitrary discontinuities without remeshing. For 3D, Lo et al. [21] developed integral equation approach for 3D multiple cracks problems, then Krysl and Belytschko [22] employed the element free Galerkin method for dynamic propagation of arbitrary 3D cracks, later Rabczuk [23] proposed a three dimensional meshfree method for continuous multiple-crack initiation, propagation and junction in statics and dynamics. Finally, Miao et al. [24–26] developed dual hybrid boundary node method for evaluating cracks in asphalt pavements.

As a new numerical method that can deal with the change from continuity to discontinuity for crack propagation process, the continuous-discontinuous cellular automaton method has been proposed by Yan, Pan and coworker [27, 28], which is based on the level set method [29], the enrichment shape function theory and discontinuous cellular automaton method [30]. In this method, the discontinuities are independent with the calculating grids, and no assembled global stiffness is needed but only cell stiffness is needed in the whole calculation.

In the present paper, a method of continuous-discontinuous cellular automaton for modeling the growth, intersection and coalescence of multiple cracks in brittle material is presented. The method uses the level set method to track arbitrary discontinuities, and calculation grids are independent of the discontinuities and no remeshing is required with the growth of crack. Based on Griffith fracture theory and Mohr–Coulumb criterion, a mixed fracture criterion for multiple crack growth in brittle material is proposed. The method treats the junction and coalescence of multiple cracks, and corresponding junction criterion and coalescence criterion for brittle material are discussed in the present work. In order to overcome the tracking error in the level set approximation for crack junction and coalescence, a dichotomy searching algorithm is proposed. Introduced the above theories into continuous-discontinuous cellular automation, the present method can be applied to solving the growth, intersection and coalescence of multiple cracks in brittle material, and only cell stiffness is needed and no assembled global stiffness is needed. Some numerical examples are given to illustrate the efficiency and accuracy of the present method for crack junction, coalescence and percolation problems.

The outline of this paper is given as follows. The theories of continuous-discontinuous cellular automaton method are presented in Sect. 2. The fracture criterion is discussed in Sect. 3. Junction and coalescence criterions are developed in Sect. 4. The numerical examples for multiple crack growth are given in Sect. 5. Finally, the paper will end with conclusions in Sect. 6.

2 Continuous-discontinuous cellular automaton method

2.1 Tracking the discontinuities

It is shown in Fig. 1 that a multiple cracks model is taken as an example, Γ_i and Γ_j are cracks. In the present method, the level set method, which is first introduced by Osher and Sethian [29], is employed to track the moving interfaces of growing cracks. The moving interface of the present method is represented as the zero level set function of $\varphi_i(\boldsymbol{x}, t)$ for crack Γ_i and $\varphi_j(\boldsymbol{x}, t)$ for crack Γ_j. Then the evolution of the moving interface can be expressed as an evolution of equation of $\varphi_i(\boldsymbol{x}, t)$ and $\varphi_j(\boldsymbol{x}, t)$ for each crack. So it can be seen that discontinuities are independent with the calculating grids and cracks are also independent with each other in whole calculation, except for an intersection is taken place. In general, a crack surface $\gamma_i(t) \subset R^2$ can be expressed as the level set curve of the function $\varphi_i(\boldsymbol{x}, t) = 0$, which is given as

$$\varphi_i(\boldsymbol{x}, t) = \xi(\boldsymbol{x}, t) = \min_{\boldsymbol{x}_{\Gamma_i} \in \Gamma(t)} \left\| \boldsymbol{x} - \boldsymbol{x}_{\Gamma_i} \right\| \cdot \text{sign}(\boldsymbol{n}^+ \cdot (\boldsymbol{x} - \boldsymbol{x}_{\Gamma_i})), \quad (1)$$

where $\boldsymbol{x}$ is the point outside of the crack surface, and $\boldsymbol{x}_{\Gamma_i}$ is

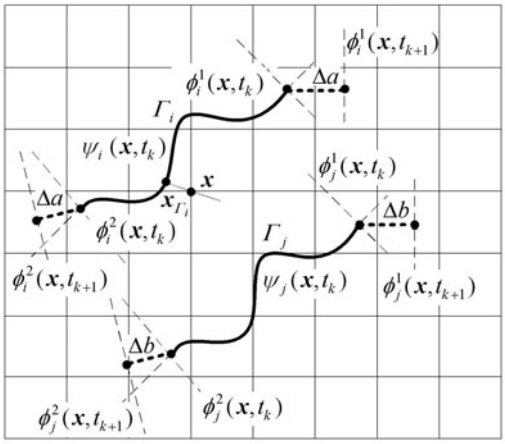

Fig. 1 Tracking model of discontinuities

any nearest point to point $\boldsymbol{x}$ on the crack surface; $\boldsymbol{n}^+$ is a unit normal vector to the crack surface.

Discretization of the level set function allows for the evaluation of the level set function at the element level based on the nodal level set values $\varphi_i^k = \varphi_i^k(\boldsymbol{x}_k, t)$ and known classical finite element shape functions $N_k(\boldsymbol{x})$ [31, 32]

$$\varphi_i(\boldsymbol{x},t) = \sum_{k=1}^{n} N_k(\boldsymbol{x},t)\varphi_i^k. \tag{2}$$

The same as the above theory, two level set functions $\phi_i^1(\boldsymbol{x},t)$ and $\phi_i^2(\boldsymbol{x},t)$ for each tip of crack Γ_i are defined, in this definition, the crack tip is represented as the intersection of the zero level set function of $\varphi_i(\boldsymbol{x},t)$ with another zero level set function of $\phi_i^1(\boldsymbol{x},t)$ or $\phi_i^2(\boldsymbol{x},t)$. So level set function $\phi_i^1(\boldsymbol{x},t)$ and $\phi_i^2(\boldsymbol{x},t)$ for the crack tips are generally assumed to be orthogonal to $\varphi_i(\boldsymbol{x},t)$ [31, 32], which is

$$\nabla\varphi_i(\boldsymbol{x},t)\nabla\phi_i^k(\boldsymbol{x},t) = 0, \quad k = 1, 2. \tag{3}$$

2.2 Enriched shape function of discontinuities

Based on partition of unity theory [27, 28] and traditional finite element shape function, the shape function for cracked element must be enriched by the Heaviside function so that the displacement and stress discontinuities caused by cracks can be exactly described, so the enriched function can be written as

$$\boldsymbol{u}^h(\boldsymbol{x}) = \sum_{j=1}^{n} N_j(\boldsymbol{x})\boldsymbol{u}_j + \underbrace{\sum_{k=1}^{m} N_k(\boldsymbol{x})(H(\xi) - H(\xi_k))\boldsymbol{a}_k}_{k\in P}, \tag{4}$$

where n and m are the node numbers of element, P is the penetrated nodes set, and the Heaviside function $H(\xi(\boldsymbol{x},t)) = \text{sign}(\xi(\boldsymbol{x},t)) = \begin{cases} 1, & \forall\xi(\boldsymbol{x},t) > 0 \\ -1, & \forall\xi(\boldsymbol{x},t) < 0 \end{cases}$.

Then the discontinuities and high gradient stresses for crack tip can be enriched by the near-tip asymptotic field functions, which is

$$\boldsymbol{u}^h(\boldsymbol{x}) = \sum_{j=1}^{n} N_j(\boldsymbol{x})\boldsymbol{u}_j + \underbrace{\sum_{i=1}^{t} N_i(\boldsymbol{x})\left(\sum_{l=1}^{nf}(F_l(\boldsymbol{x}) - F_l(\boldsymbol{x}_i))\boldsymbol{b}_i^l\right)}_{i\in T}, \tag{5}$$

where t is node number associated with crack tip node set T; nf is the number of the near-tip asymptotic field functions; $\boldsymbol{b}_i^l$ is a vector of additional nodal freedom, $\{F_l(\boldsymbol{x}), l = 1-4\} = \left\{\sqrt{r}\sin\left(\frac{\theta}{2}\right), \sqrt{r}\cos\left(\frac{\theta}{2}\right), \sqrt{r}\sin(\theta)\sin\left(\frac{\theta}{2}\right), \sqrt{r}\sin(\theta)\cos\left(\frac{\theta}{2}\right)\right\}$, in which r and θ are coordinates of polar coordinate of crack tip, which can be seen in Ref. [27].

2.3 Crack surface and model

As we all know, under compression loading, the crack may be at close state, and there are normal and tangential stresses on crack surfaces. So frictional contact model for the present method is employed, which can be seen in Fig. 2. Assuming that the displacement and traction on each face of the crack surfaces are: $\boldsymbol{w}^{\mathrm{S}}, \boldsymbol{t}^{\mathrm{S}}$ on Γ_{S} and $\boldsymbol{w}^{\mathrm{T}}, \boldsymbol{t}^{\mathrm{T}}$ on Γ_{T}, and they satisfy

$$\boldsymbol{t}^{\mathrm{S}} = -\boldsymbol{t}^{\mathrm{T}}, \quad \boldsymbol{w}^{\mathrm{S}} = \boldsymbol{u}|_{\Gamma_{\mathrm{S}}}, \quad \boldsymbol{w}^{\mathrm{T}} = \boldsymbol{u}|_{\Gamma_{\mathrm{T}}} \quad \text{on crack surface.} \tag{6}$$

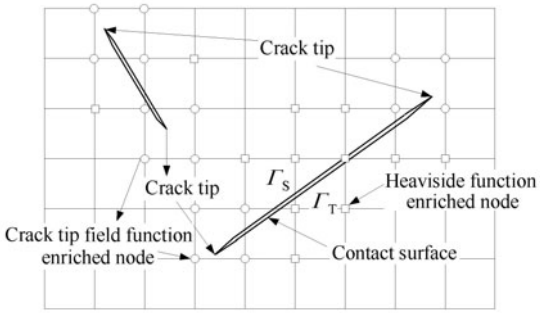

Fig. 2 Crack surface and crack model

According to kinematics, equilibrium, the constitutive laws and fictional contact theory, the variational formulation can be expressed as [27, 28]

$$\int_{\Omega}\boldsymbol{\sigma}:\nabla^{\mathrm{S}}\boldsymbol{u}^*\mathrm{d}\Omega = \int_{\Omega}\boldsymbol{b}\cdot\boldsymbol{u}^*\mathrm{d}\Omega + \int_{\Gamma_{\mathrm{t}}}\bar{\boldsymbol{t}}\cdot\boldsymbol{u}^*\mathrm{d}s + \int_{\Gamma_{\mathrm{s}}}\boldsymbol{t}\cdot\boldsymbol{w}^*\mathrm{d}s. \tag{7}$$

The superscript "*" denotes the weight function. And the last term of Eq. (7) can be rewritten as [27, 28]

$$\int_{\Gamma_{\mathrm{d}}}\boldsymbol{t}\cdot\boldsymbol{w}^*\mathrm{d}s = \int_{\Gamma_{\mathrm{S}}}\boldsymbol{t}^{\mathrm{S}}\cdot\boldsymbol{w}^{\mathrm{S}^*}\mathrm{d}s + \int_{\Gamma_{\mathrm{T}}}\boldsymbol{t}^{\mathrm{T}}\cdot\boldsymbol{w}^{\mathrm{T}^*}\mathrm{d}s = \int_{\Gamma_{\mathrm{d}}}\boldsymbol{t}^{\mathrm{S}}\cdot\tilde{\boldsymbol{u}}\mathrm{d}s. \tag{8}$$

In which $\tilde{\boldsymbol{u}} = \boldsymbol{w}^{\mathrm{S}} - \boldsymbol{w}^{\mathrm{T}}$.

According to the enriched shape functions of Eqs. (4) and (5), we can get the relative displacement between crack surfaces Γ_{S} and Γ_{T} [27]

$$\tilde{\boldsymbol{u}} = \underbrace{2\sum_{k=1}^{m} N_k(\boldsymbol{x})\boldsymbol{a}_k}_{k\in P} + \underbrace{2\sum_{i=1}^{t} N_i(\boldsymbol{x})\sqrt{r}\boldsymbol{b}_i^0}_{i\in T} = \tilde{\boldsymbol{N}}\{\boldsymbol{a},\boldsymbol{b}\}^{\mathrm{T}}. \tag{9}$$

In which $\tilde{\boldsymbol{N}}$ is the shape function that related to the relative displacement between two crack surfaces of a crack.

According to frictional contact theory, we assume that $g_N(\boldsymbol{x})$ and $g_T(\boldsymbol{x})$ are the normal and tangential gap between two contact surfaces, and $\boldsymbol{p}_N$ and $\boldsymbol{p}_T$ are contact stresses in normal and tangential direction. According to Coulomb frictional contact model, their relation can be given as

$$\begin{aligned} &\boldsymbol{p}_N = k_N g_N(\boldsymbol{x})\boldsymbol{n}(\boldsymbol{x}), \quad && g_N(\boldsymbol{x}) \leqslant 0, \\ &\boldsymbol{p}_N = \boldsymbol{0}, && g_N(\boldsymbol{x}) > 0, \end{aligned} \tag{10}$$

$$F_c(\boldsymbol{p}, u) = \|\boldsymbol{p}_T\| - \mu_c \|\boldsymbol{p}_N\| - c_c \begin{cases} = 0, & \text{slip}, \\ < 0, & \text{adherence}, \end{cases} \tag{11}$$

where $\boldsymbol{n}(\boldsymbol{x})$ is outward normal vector of crack surface, and k_N is normal stiffness of crack surface, and μ_c and c_c are the coefficient of friction and tangential cohesion of crack surface respectively.

According to cohesion contact model, their relation can be given as

$$\begin{aligned} &\boldsymbol{p}_N = k_N g_N(\boldsymbol{x})\boldsymbol{n}(\boldsymbol{x}), && g_N(\boldsymbol{x}) \leqslant 0, \\ &\boldsymbol{p}_N = k_C(g_C - g_N(\boldsymbol{x}))\boldsymbol{n}(\boldsymbol{x}), && 0 < g_N(\boldsymbol{x}) \leqslant g_C, \\ &\boldsymbol{p}_N = \boldsymbol{0}, && g_N(\boldsymbol{x}) > g_C, \end{aligned} \tag{12}$$

$$\begin{aligned} &\boldsymbol{p}_T = (\mu_c \|\boldsymbol{p}_N(\boldsymbol{x})\| + c_c)\boldsymbol{t}(\boldsymbol{x}), \quad && g_N \leqslant 0, \\ &\boldsymbol{p}_T = \boldsymbol{0}, && g_N > 0, \end{aligned} \tag{13}$$

where k_C is the stiffness related to the cohesion, and g_C is critical value of relative gap between crack surfaces.

Substituting Eqs. (4), (5), and (9) into Eqs. (7) and (8), we can obtain

$$\boldsymbol{K}_{ij} = \begin{bmatrix} \boldsymbol{K}_{ij}^{uu} & \boldsymbol{K}_{ij}^{ua} \\ \boldsymbol{K}_{ij}^{au} & \boldsymbol{K}_{ij}^{aa} + \boldsymbol{K}_{ij}^{I} \end{bmatrix}, \quad \boldsymbol{f}_i = \left\{ \boldsymbol{f}_i^u,\ \boldsymbol{f}_i^a - \boldsymbol{f}_i^I \right\}, \tag{14}$$

where

$$\boldsymbol{K}_{ij}^{\alpha\beta} = \int_{\Omega^e} (\boldsymbol{B}_i^\alpha)^T \boldsymbol{D} (\boldsymbol{B}_j^\beta) \mathrm{d}\Omega,$$

$$\boldsymbol{K}_{ij}^{I} = \int_{\Gamma_S} (\tilde{\boldsymbol{N}}_i)^T (\boldsymbol{D}_f^e)(\tilde{\boldsymbol{N}}_j) \mathrm{d}\Gamma,$$

$$\boldsymbol{f}_i^I = \int_{\Gamma_S} \tilde{N}^T \boldsymbol{t}_S \mathrm{d}\Gamma,$$

$$\boldsymbol{f}_i^\alpha = \int_{\Gamma^e} N_i^\alpha \bar{\boldsymbol{t}} \mathrm{d}\Gamma + \int_{\Omega^e} N_i^\alpha \boldsymbol{f} \mathrm{d}\Omega,$$

in which $\alpha, \beta = u, a$, $\boldsymbol{D}$ is the elasto-plastic constitutive matrix of rock, and $\boldsymbol{D}_f^e$ is constitutive matrix related to contact, $\boldsymbol{B}_i^\alpha$ is derivative matrix of traditional finite element shape function matrix, and the detailed formulation can be seen in Ref. [27]. In the present method, only the brittle material is considered, and when cracks growth together or reach the boundary, the plastic zones are not considered, so only linear elastic concept is given in this section.

According to Eq. (14), we assume that residual force of cell i is $\boldsymbol{r}_i$, which can be written as

$$\boldsymbol{r}_i = \begin{Bmatrix} \boldsymbol{f}_i^u \\ \boldsymbol{f}_i^a + \boldsymbol{f}_i^I \end{Bmatrix} - \boldsymbol{K}_{ii}\boldsymbol{d}, \quad \boldsymbol{d} = \{\boldsymbol{u}_i, \boldsymbol{a}_i\}^T. \tag{15}$$

In Eq. (15), $\boldsymbol{f}_i^I$ is unknown, because contact forces $\boldsymbol{t}_S$ is unknown in every cell. Then, at each node, we use Newton's iteration method, we can get

$$\boldsymbol{d}_{n+1} = \boldsymbol{d}_n - \frac{\boldsymbol{r}_i(\boldsymbol{d}_n)}{\boldsymbol{r}_i'(\boldsymbol{d}_n)}, \tag{16}$$

where $\boldsymbol{r}_i'(\boldsymbol{d}_n)$ is derivative of $\boldsymbol{r}_i(\boldsymbol{d}_n)$, n is iteration step. For this iteration, firstly, we assume that $\boldsymbol{d}_0 = \boldsymbol{0}$ and $\boldsymbol{t}_S^0 = \boldsymbol{0}$ at first step, then we can get $\boldsymbol{d}_1$ and $\boldsymbol{t}_S^1$, and so on, the iteration is done until $\boldsymbol{r}_i \to \boldsymbol{0}$ is satisfied.

2.4 Continuous and discontinuous cellular automaton (CDCA)

Through CDCA, the equilibrium state of a cell can be obtained by the one-another transfer of the information between cells. The behavior of a cell is thought to be essentially local. There are three advantages for this theory. One is no need to assemble the global matrix. The second is that it is easy to consider the local properties of material. The third one is that the easy implementation of parallel algorithm.

2.4.1 Cell space and its state

Cell model includes the continuous cell and discontinuous cell. The cell consists of cell nodes N_i, corresponding cell elements E_i^j and its neighbor cell nodes N_i^k, in which cell nodes include classical finite element nodes, the Heaviside enriched nodes and the near-tip asymptotic field function enriched nodes and elements consist of classical finite elements, penetrated elements and crack tip elements.

Physical and mechanical values of cell are determined by the cell state, which is shown in Fig. 3, it is composed of the degree value vector of nodal freedom $\boldsymbol{u}^h = \{u, a, b\}$, in which u is traditional degree of nodal freedom, a is the Heaviside enriched degree of nodal freedom and b is crack tip field function enriched degree of nodal freedom; material property of thickness t, Young's modulus E, Poisson's ratio μ and fracture toughness K_{IC}; cell nodal forces vector $\boldsymbol{f} = \{\boldsymbol{f}_u, \boldsymbol{f}_a, \boldsymbol{f}_b\}$, in which the subscript u, a and b are represented traditional, the Heaviside enriched and the near-tip asymptotic field functions enriched degrees of nodal freedom respectively; elastic strain ε_e, equivalent plastic strain ε_p and equivalent stress intensity factor K_{Ie}, contact states c_s and contact stresses t_N and t_T and so on.

2.4.2 Continuity to discontinuity model

In CDCA model, the discontinuity may exist in some cellular elements, which can be seen in Fig. 4. The location of crack will determine the cellular node type, cellular element type and cellular automaton model. And in this method, the crack path is tracked by the level set functions. By way of the values of the level set functions, the node cellular type,

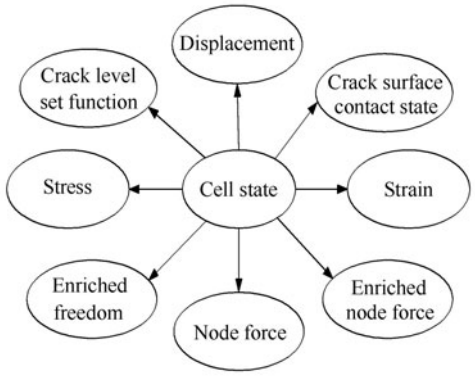

Fig. 3 Cell states

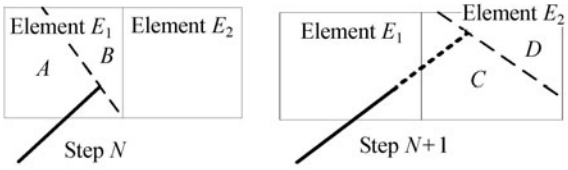

Fig. 4 Continuity to discontinuity model

element cellular type and cellular automaton model are updated, especially for some cells, which change from continuous cellular automaton model to discontinuous cellular automaton model.

2.4.3 Updating rule

Considering a cell node N_i for a plane elastic problem, the displacement of this cell node can be obtained due to the effect of nodal force vector $\boldsymbol{f}_i = \{\boldsymbol{f}_i^u, \boldsymbol{f}_i^a, \boldsymbol{f}_i^b\}$ when restricted all degrees of nodal freedoms on its neighbor cell nodes N_i^k, which can be shown in Fig. 5. The relation between the incremental force and incremental deformation can be reflected into two steps. Firstly, the nodal force increment $\Delta\boldsymbol{f}_i = \{\Delta\boldsymbol{f}_i^u, \Delta\boldsymbol{f}_i^a, \Delta\boldsymbol{f}_i^b\}$ will lead the cell node N_i to produce the displacement increment $\Delta\boldsymbol{u}_i^h = \{\Delta\boldsymbol{u}_i, \Delta\boldsymbol{a}_i, \Delta\boldsymbol{b}_i\}$. Then, the displacement increment $\Delta\boldsymbol{u}_i^h$ on the cell node N_i will lead its neighboring cell nodes N_i^k to produce the nodal force increment $\Delta\boldsymbol{f}_i^k$.

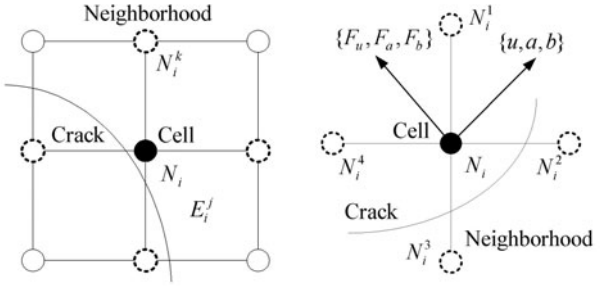

Fig. 5 Updating model

Therefore, the process of CDCA updating rules is: increment of nodal force leads to the increment of nodal displacement, and the increment of nodal displacement leads to the increment of nodal force for its neighboring nodes, until the system static equilibrium is achieved, in other words, $\Delta\boldsymbol{u}_i^h \to \boldsymbol{0}$ and $\Delta\boldsymbol{f}_i^k \to \boldsymbol{0}$ appear. So the updating rule can be given as:

(1) The equilibrium equation of cell N_i can be described as $\boldsymbol{K}_i\Delta\boldsymbol{u}_i^h = \Delta\boldsymbol{f}_i$, in which $\boldsymbol{K}_i$ is the stiffness of cell N_i, $\Delta\boldsymbol{u}_i^h = \{\Delta\boldsymbol{u}_i, \Delta\boldsymbol{a}_i, \Delta\boldsymbol{b}_i\}$, $\Delta\boldsymbol{f}_i = \{\Delta\boldsymbol{f}_i^u, \Delta\boldsymbol{f}_i^a, \Delta\boldsymbol{f}_i^b\}$ are increment of degrees of nodal freedom and nodal force of cell N_i respectively.

(2) Restricting all degrees of nodal freedom on all neighboring cells N_i^k, which can be seen in Fig. 5, and calculating the increment of degrees of nodal freedom $\Delta\boldsymbol{u}_i^h$ via the increment of nodal force $\Delta\boldsymbol{f}_i$.

(3) Obtaining the nodal force increment $\Delta\boldsymbol{f}_i^k$ of the neighboring cell N_i^k via $\Delta\boldsymbol{u}_i^h$ from equation $\Delta\boldsymbol{f}_i^k = \boldsymbol{K}_i^k\Delta\boldsymbol{u}_i^h$, Where $\boldsymbol{K}_i^k$ is the stiffness of neighboring cell N_i^k.

(4) Finishing the calculation of steps (1)–(3) on all cell nodes, until $\Delta\boldsymbol{u}_i^h \to \boldsymbol{0}$ and $\Delta\boldsymbol{f}_i^k \to \boldsymbol{0}$ appear.

(5) According to the displacement results of step (4), calculating the normal pressure of crack surface $\boldsymbol{p}_\mathrm{N}$ via Eqs. (10) or (12). Obtaining trial tangential pressure $\boldsymbol{p}_\mathrm{T}^\mathrm{trial} = k_\mathrm{T}g_\mathrm{T}(\boldsymbol{x})\boldsymbol{t}(\boldsymbol{x})$, in which k_T is tangential stiffness of contact surface. And define a trial function $\phi^\mathrm{trial} = \left\|\boldsymbol{p}_\mathrm{T}^\mathrm{trial}\right\| - \|\mu_\mathrm{c}\boldsymbol{p}_\mathrm{N}\|$.

(6) If trial function $\phi^\mathrm{trial} < 0$ (stick), $\boldsymbol{p}_\mathrm{T} = \boldsymbol{p}_\mathrm{T}^\mathrm{trial}$, and go to step (7); if trial function $\phi^\mathrm{trial} > 0$ (slip), $\boldsymbol{p}_\mathrm{T} = -\mu_\mathrm{c}\|\boldsymbol{p}_\mathrm{N}\|\boldsymbol{t}(\boldsymbol{x})$, and go to step (1).

(7) According to steps (1)–(4), calculating iteration residual $\boldsymbol{r}$ of Eq. (14), if $\|\boldsymbol{r}\| < toler$, iteration finishes, otherwise, updating initial value and return to step (1).

It is shown in this section, the whole calculation is focused on cell, so no assembled global stiffness is needed, but only node stiffness is required, which can greatly save the computer memory, and it is easy to consider the local properties of material because of its local property of the present method.

3 Mixed fracture criterion

Crack propagation in brittle material, especially for rock material, are almost caused by tensile stress and shear stress, for example, a rock under compression and shearing load, the crack may propagate when the tensile stress is beyond its tensile strength or the shear stress is beyond its shear strength. The maximum circumferential tensile stress criterion is a famous fracture criterion, and it is suitable for Mode I fracture [33, 34], but for shearing fracture it is not suitable for some special cases, especially for shear failure for rock material. So a mixed fracture criterion must be constructed for tensile fracture and shearing fracture of brittle material.

3.1 Tensile fracture and combination fracture of tension and shear

According to Griffith theory, when the circumferential tensile stress is larger than the tensile strength of material, the

fracture starts, and the crack growing criterion can be given as

$$\sigma \geqslant \sigma_{\mathrm{T}}, \quad 3\sigma_1 + \sigma_3 \geqslant 0, \tag{17}$$

$$(\sigma_1 - \sigma_3)^2 = -8\sigma_{\mathrm{T}}(\sigma_1 + \sigma_3), \quad 3\sigma_1 + \sigma_3 < 0, \tag{18}$$

where σ_{T} is the tensile strength of material, and σ_1, σ_2 are principle stress on any point of crack tip.

According to Eqs. (17) and (18), the above equation can be rewritten as

$$\tau^2 = 4\sigma_{\mathrm{T}}(\sigma_{\mathrm{T}} - \sigma_{\mathrm{n}}). \tag{19}$$

So at fracture angle θ, Eq. (19) is satisfied, the crack propagation occurs.

3.2 Shearing fracture

In addition, for the influence of shear stress, a shearing failure occurs when the Mohr–Coulumb criterion is satisfied, which can be given as

$$\mathrm{Max}\,[\tau_{\mathrm{rn}}(r_0, \theta_0)] \geqslant \sigma_{\mathrm{n}}(r_0, \theta_0)\mathrm{tg}\varphi + c, \tag{20}$$

where $\sigma_{\mathrm{n}}(r_0, \theta_0)$ is the compression on normal direction of crack propagating direction, and φ is friction angle of material, c is cohesion of material. In other words, shearing fracture occurs at an angle $\theta = \theta_0$, and at the point with $\theta = \theta_0$ and $r = r_0$, the shear stress τ_{rn} is the maximum, which can be seen in Fig. 6, and the shear stress on this point satisfies Mohr–Coulomb criterion: $\tau_{\mathrm{rn}}(r_0, \theta_0) \geqslant \sigma_{\mathrm{n}}(r_0, \theta_0)\mathrm{tg}\varphi + c$.

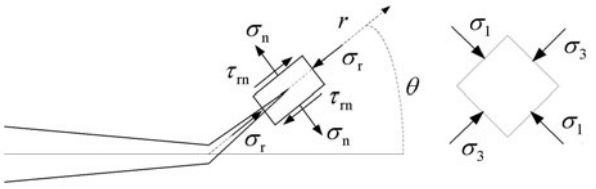

Fig. 6 Crack tip stress field model

Actually, the tensile facture is always a priority one for brittle material.

3.3 Propagating step

According to this propagating criterion, the propagating step is defined as: (1) for tensile fracture, the crack arrest point is located at the point $\sigma_1 = \sigma_{\mathrm{T}}$ on its growth path, and the propagating step is the length between crack tip and crack arrest point. Based on this theory, the propagating step is always different on different steps; (2) for shearing fracture, the crack arrest point is located at the point $\tau_{\mathrm{rn}}(r_0, \theta_0) = \sigma_{\mathrm{n}}(r_0, \theta_0)\mathrm{tg}\varphi + c$, and the same as tensile fracture, the propagating step is the length between crack tip and crack arrest point.

4 Junction and coalescence criteria

Multiple crack growth must deal with several situations, such as the junction, coalescence of cracks and growth to reach a boundary and so on, when they are junction, especially for one crack growth reaching another crack, the positional relationship between those two cracks may occur error in the process of the level set approximation. So some algorithms are developed for those situations in this section.

4.1 Growth to reach a boundary

Crack tips that are identified to grow are treated separately when they reach a free boundary. When this occurs, one must kill the crack tip and let the crack tip terminate on the free boundary, and at the same time, this crack tip is no longer a crack tip. At this time the enrichment function of Eq. (5) for this crack tip must be eliminated, and the Heaviside function enriched shape function of Eq. (4) is used to replace the enrichment function of crack tip.

When a crack tip is growing to cross a free boundary, we must check the positional relationship among cracks, discontinuities and free boundaries. It is shown in Fig. 7, at step i, when the crack tip A is growing, the possible crack tip of current step can be B, C or D, if growing path is along AB or AC, no special treatment is required. But the smallest distance from crack tip A to free boundary is AE, if the distance $d_i < \Delta a_i$, in which Δa_i is the growth increment on current growing step, so we assume that the crack growing path on current step is along AD, and the crack terminates on the boundary at point E, and the crack end of E is no longer crack tip.

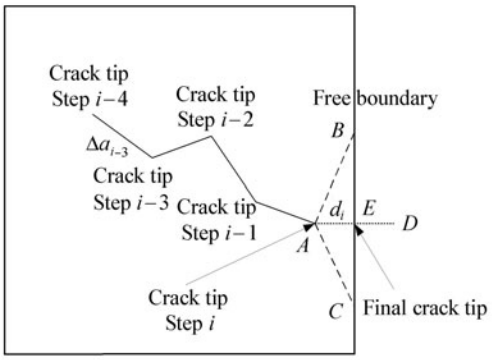

Fig. 7 Crack tip reaching a free boundary

4.2 Crack junction

When a crack grows to reach another crack, a crack junction is taken place, and the enriched shape function must be changed to suit this case.

4.2.1 Crack connection

If two crack tips for different cracks are very close at step i, and at $i+1$ step they are both growing. If they propagate separately, at the same step $i+1$ they may intersect, which can be seen in Fig. 8. A_1 is the crack tip of crack 1 at current step, and A_2 is the crack tip of crack 2 at current step, and they

both propagate on current step, and the possible new crack tip of crack 1 is B_1, and the possible new crack tip of crack 2 is B_2. It is obvious that they intersect at current step. On this case, we consider that crack connection occurs. At this time, both crack 1 and crack 2 is going to grow to the final crack tip E, and they connect together to form one crack. And the new crack tip E for both cracks is no longer crack tip.

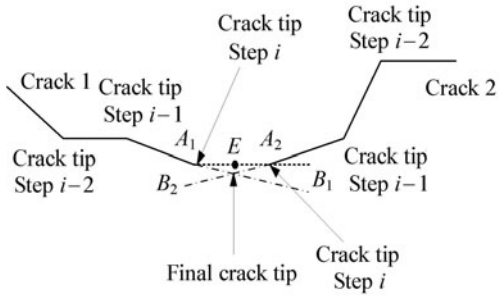

Fig. 8 Crack connection

4.2.2 Crack coalescence

When a crack is growing to reach another crack, a junction between two cracks occurs, which can be seen in Fig. 9, and in this work a crack coalescence is allowed, which is almost the same as Ref. [20].

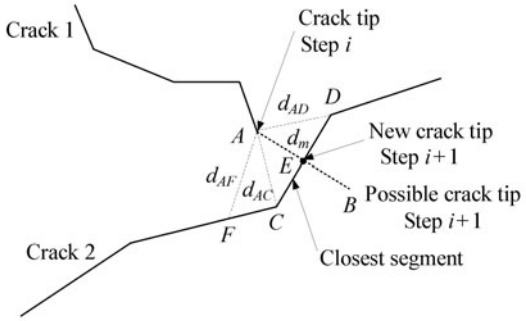

Fig. 9 Model of crack coalescence

It is shown in Fig. 9, when crack tip A of crack 1 is very close to another crack, we must check the distance from crack tip A to another crack surface, and the closest segment of crack 2 can be get, which is closest to crack tip A, and the smallest distance is d_m, if $d_m < \Delta a_i$, in which Δa_i is the growth increment on current growing step. Then we assume that the crack tip A is growing along path AB, and terminates on crack 2 at point E. On this case, the cracks are joined, and E is no longer the crack tip of crack 1, and the crack tip enrichment is removed from old setting, and new junction enrichment must be added. In addition, an examination must be performed to avoid the creation of a rigid body mode when the coalescence occurs.

4.2.3 Junction enrichment

When a junction occurs, the enrichments of Eqs. (4) and (5) can not exactly describe the discontinuous displacements, so a new enrichment must be developed. At this time, the enrichment is similar to Ref. [20]. At junction element, the enrichment can be given as [20]

$$\boldsymbol{u}^h(\boldsymbol{x}) = \sum_{j=1}^{n} N_j(\boldsymbol{x})\boldsymbol{u}_j + \underbrace{\sum_{k=1}^{m_1} N_k(\boldsymbol{x}) J_j^m \boldsymbol{a}_j^m}_{k\in J^m} + \underbrace{\sum_{l=1}^{m_2} N_l(\boldsymbol{x}) J_l^M \boldsymbol{a}_l^M}_{k\in J^M}, \tag{21}$$

where J is the junction enrichment of crack m, and its form is [20]

$$J_j^m(\boldsymbol{x}) = \begin{cases} H(f^m(\boldsymbol{x})) - H(f^m(\boldsymbol{x}_J)), & \boldsymbol{x} \in A, \\ H(f^M(\boldsymbol{x})) - H(f^M(\boldsymbol{x}_J)), & \boldsymbol{x} \in B, \end{cases} \tag{22}$$

where A and B are different areas divided by crack m and M, and $f^m(\boldsymbol{x})$ and $f^M(\boldsymbol{x})$ are the level set function of crack m and M, which can be seen in Fig. 10.

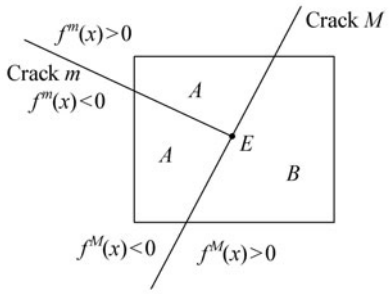

Fig. 10 Model of junction element

4.2.4 Dichotomy searching algorithm

It is shown in Fig. 9 that crack 1 and crack 2 intersect at point E, in other words, crack 1 terminates at point E on crack 2, but those positional relationships are stored as the level set function on nodes, unfortunately after the level set approximation by the level set method, this positional relationship may be changed because of the error of approximation, which can be seen in Fig. 11. Then a dichotomy searching algorithm is developed in this method to overcome this defect. It is shown in Fig. 11 that crack 1 terminates at point E_1 but not at crack 2 after the level set approximation of those two cracks, and crack 1 may pass through crack 2 at point E_1 in Fig. 11b, or crack 1 may not intersect with crack 2 and terminate at point E_1 in Fig. 11c.

We can see that both Figs. 11b and 11c can not reflect the exact positional relationship of crack 1 and crack 2. In order to overcome this problem, a dichotomy searching algorithm is developed in this paper, which can be seen in Fig. 12. And the dichotomy searching algorithm for the present method is given as:

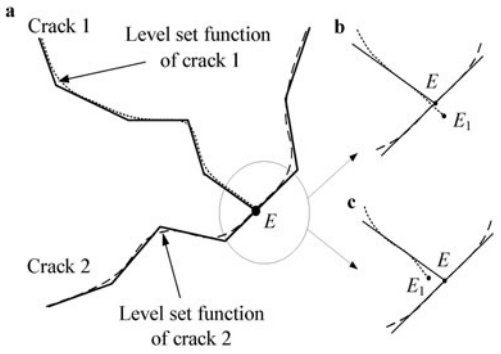

Fig. 11 Level set model of multiple cracks

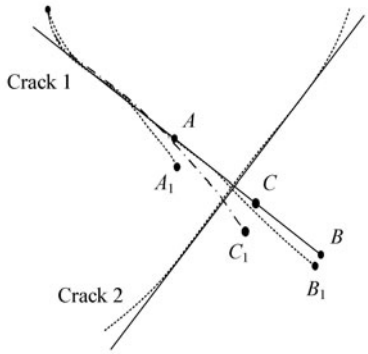

Fig. 12 Dichotomy searching algorithm model

Step 1. Check the approximat results of the level set approximation, if an error is made such as Fig. 11, the dichotomy searching algorithm is applied. Does the level set approximation for crack 2, and in the following we use a new crack shape via the level set approximation as crack 2.

Step 2. Search a point A at crack 1, and assume that this point is the end of crack 1, at this time crack 1 can not reach crack 2, and the level set function of crack 1 end with point A can not reach crack 2. After the level set approximation, A_1 is the end of crack 1, and can also not reach crack 2.

Step 3. Search another point B on extent line of crack 1, and assume that this point is the end of crack 1, on this case crack 1 intersects with crack 2 at point E, and the level set function of crack 1 can also intersect with crack 2, after level set approximation, B_1 is the end of crack 1, and crack 1 can also pass through crack 2.

Step 4. Via point A and B of crack 1, get the midpoint C of line AB, in addition, get its corresponding point C_1 by the level set approximation. Assuming that C is the end of crack 1, if crack 1 passes through crack 2 after the level set approximation, use the point C to replace the point B, and continue step 4, if crack 1 can not reach crack 2 after the level set approximation, use the point C to replace the point A, and continue step 4, if C_1 is fortunately located on crack 2, end step 4.

Step 5. Use point C as the end of crack 1, and do the level set approximation for crack 1, and after the dichotomy searching algorithm optimization, the positional relationship of those two cracks can be exactly reflected.

5 Numerical examples

5.1 Studies of computational accuracy and efficiency

In this section, consider an edge-cracked plate under pure tension as an example, that the length, $2D = 20$ mm, and width, $L = 52$ mm, and the crack length $a = 12$ mm. The far field tensile stress, $\sigma = 0.2$ GPa, and the material property are given as: $E = 76$ GPa, $\mu = 0.286$, in which the results are compared with those in Ref. [35].

5.1.1 Stress accuracy

The σ_x and σ_y near crack tip are given in Fig. 13, in which the analytical results and those obtained by numerical manifold method (NMM) [35] are given for comparison. It is shown in those figures that a good agreement is achieved between those results, and in the present method a total of 4 017 elements are used.

5.1.2 Comparison of computer memory

Figure 14 plots the computer memory comparison between the present method and extended finite element method (XFEM), and in XFEM a half-bandwidth storage technique is used. It can be seen that much less computer memory is needed in the present method

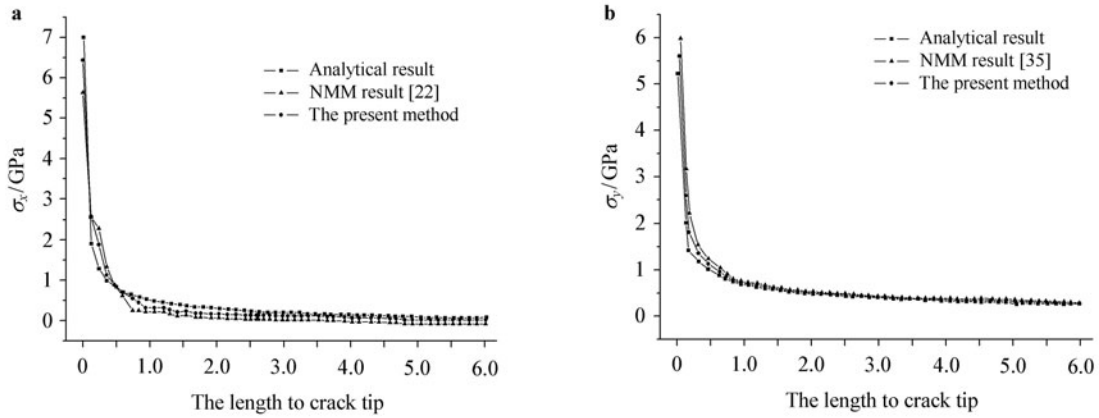

Fig. 13 Stress comparison of the present method. **a** σ_x at the tip of the crack; **b** σ_y at the tip of the crack

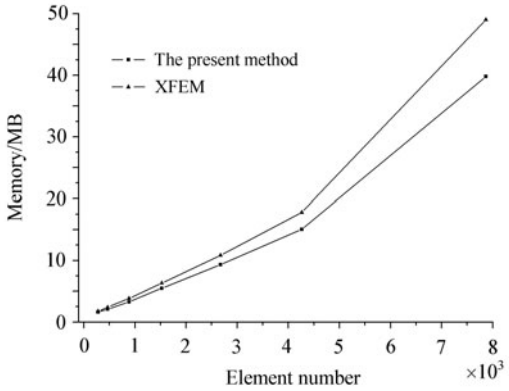

Fig. 14 Computer memory comparison between XFEM and the present method

than that of XFEM with half-bandwidth storage technique, and which is much more obvious when the element number is much larger, the reason for which is that the calculations is only located on each node, and no assembled matrix is needed in the whole calculation in the present method, but for XFEM, an assembled global stiffness matrix is inevitable, so the computer memory expanse is much larger for XFEM. According to the studies of computational time consumption of the present method, we can see that the present method is a little time-consuming than that of XFEM, which can be referred to Ref. [27], and which will be improved via the development of the parallel version of the present method.

5.2 Two cracks coalescence

Some experimental and numerical studies for multiple crack propagation under compression and shearing load have been done by a lot of researchers, in order to test the present method, the present method results are compared with experimental results by Wong [36] and numerical results by Zhou [37]. Wong et al. [36] used a mixture of the modeling material, which are composed of barite, sand, plaster and water. The material proprieties are given as: E = 0.33 GPa, ν = 0.19, σ_c = 2.09 MPa, σ_t = 0.35 MPa, K_{IC} = 0.044 3 MPa·m$^{1/2}$, k_N = 40 GPa, k_T = 0.4 GPa, μ_c = 0.45. The geometry of cracked plate can be seen in Fig. 15, and the dimensions of specimens containing two cracks are 120 mm × 60 mm, and the length of crack is a = 12 mm and the distance between two cracks is a = 20 mm, crack inclination is 45°, and in present method, a total of 16 471 elements are used, and a total of 16 744 nodes are used.

It is shown in Fig. 16 the present method results of two cracks coalescence are given, and results by Wong [36] and Zhou [37] in Fig. 15 are also given for comparison. In Fig. 16 thick solid lines are original cracks and thin dot lines are fracturing paths, and in this method we give a fixed length of expansion step for each growing step, and the length of expansion step is small enough. It can be seen in those figures that the present method results are very close to the experimental results by Wong [36] and numerical results by Zhou [37], and they illustrate that the present method is efficient and accurate. It also reveals that the coalescence criterions proposed in the present work are suitable.

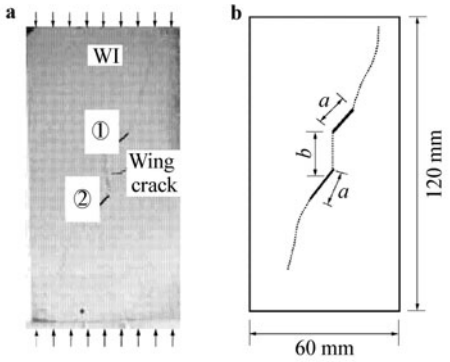

Fig. 15 Photographs of model tests [36, 37]. **a** Experiment figure; **b** Sketch of experimental results

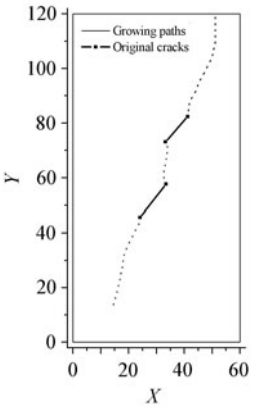

Fig. 16 Fracture paths of the present method simulation results

5.3 Three cracks coalescence

Consider a rock specimen with its dimensions are 30 mm × 15 mm, and contains 3 cracks and the length of each crack is 3 mm, which can be seen in Fig. 17, and we look the present experiment as a plane stress problem. The material proprieties are given as [38, 39]: Young's modulus of rock specimen E = 47.8 GPa; Poisson's ratio ν = 0.25; cohesive strength 15 MPa, internal friction angle 49°; tensile strength σ_T = 3.24 MPa; fracture toughness of K_{IC} = 1.03 MPa·m$^{1/2}$, K_{IIC} = 2.52 MPa·m$^{1/2}$. Normal stiffness and tangential stiffness of crack surface are given as k_N = 200 GPa and k_T = 20 GPa, and the coefficient of friction of crack surface is given as μ_c = 0.50. And in the present method, a total of 20 301 elements are used, and a total of 20 604 nodes are used.

It is shown in Figs. 18 and 19 that the experimental results and EPCA simulating results by the group of Feng [39] are given for comparison. The present method results are given in Fig. 20, it can be seen in those figures that the simulating results by the present method are very close to the results of experiment and EPCA. In which the growing paths of multiple cracks are very close with each others.

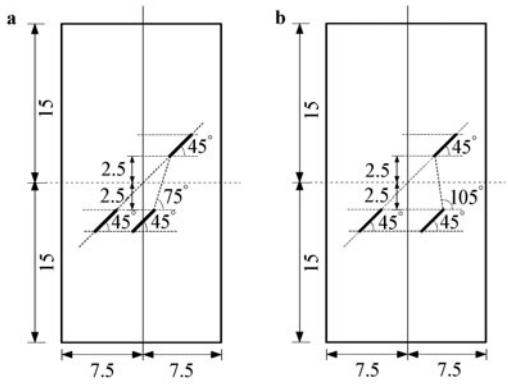

Fig. 17 Three cracks coalescence model of rock specimen [39]. **a** Case 1; **b** Case 2

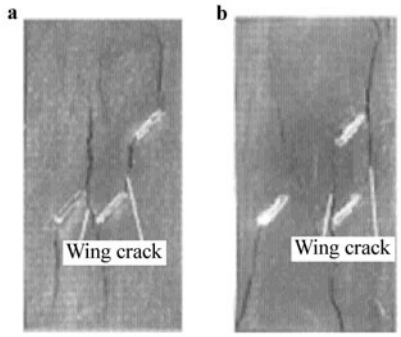

Fig. 18 Experimental results of three crack coalescence [38, 39]. **a** Case 1; **b** Case 2

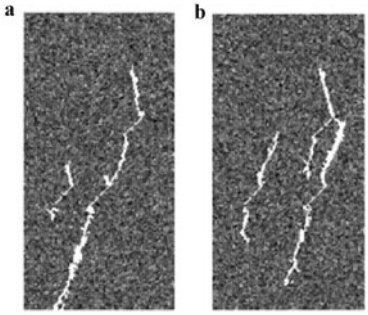

Fig. 19 EPCA results of three crack coalescence [39]. **a** Case 1; **b** Case 2

6 Conclusion

In the present paper, a method of continuous-discontinuous cellular automaton for modeling the growth of multiple cracks in brittle material is presented. The method uses the level set method to track arbitrary discontinuities, and calculation grids are independent with the discontinuities and no remeshing is required as the cracks growing. Based on cellular automaton method, only cell stiffness is needed and no assembled global stiffness is needed in the whole calculation. In all, there are four aspects of development for this paper, which are concluded as:

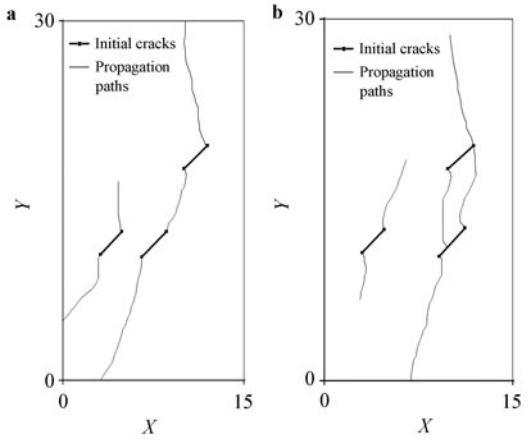

Fig. 20 CDCA results of three crack coalescences. **a** Case 1; **b** Case 2

(1) Discontinuous cellular automaton model for multiple cracks, and contact model for multiple cracks are developed in the present work.

(2) Based on Griffith fracture theory and Mohr–Coulumb criterion, a mixed fracture criterion for multiple crack growth in brittle material is developed, which is suitable for brittle material, such as rock, concrete and so on.

(3) The present work treats the junction and coalescence of multiple cracks, and corresponding junction criterion and coalescence criterion for brittle material are presented in the present work.

(4) A dichotomy searching algorithm is proposed to overcome the tracking error in level set approximation for crack junction and coalescence.

Introduced the above theory into continuous-discontinuous cellular automaton, the present method is applied to solve multiple crack growth in brittle material. Some numerical examples are given to show that the present method is efficient and accurate for crack junction, coalescence and percolation problems.

References

1 Tanaka, K., Akiniwa, Y., Shimizu, K.: Propagation and closure of small cracks in SiC particulate reinforced aluminum alloy in high cycle and low cycle fatigue. Engineering Fracture Mechanics **55**, 751–762 (1996)

2 Lawler, J.: Hybrid fiber-reinforcement in mortar and concrete. [Ph.D. Thesis]. Department of Civil and Environmental Engineering, Northwestern University, USA (2001)

3 Barpi, F., Valente, S.: Size-effects bifurcation phenomena during multiple cohesive crack propagation. International Journal of Solids and Structures **35**, 1851–1861 (1998)

4 Datsyshin, A.P., Savruk, M.P.: A system of arbitrarily oriented cracks in elastic solids. Journal of Applied Mathematics and Mechanics **37**, 306–332 (1973)

5 Kachanov, M.: Elastic solids with many cracks: A simple

method of analysis. International Journal of Solids and Structures **23**, 23–43 (1987)
6 Kachanov, M.: A simple technique of stress analysis in elastic solids with many cracks. International Journal of Fracture **28**, R11–R19 (1985)
7 Rubinstein, A.: Macrocrack interaction with semi-infinite microcrack array. International Journal of Fracture **27**, 113–119 (1985)
8 Rubinstein, A.: Macrocrack-mircodefect interaction. Journal of Applied Mechanics **53**, 505–510 (1996)
9 Freij-Ayoub, R., Dyskin, A.V., Galybin, A.N.: The dislocation approximation for calculating crack interaction. International Journal of Fracture **86**, L57–L62 (1997)
10 Chen, Y.Z.: General case of multiple crack problems in an infinite plate. Engineering Fracture Mechanics **20**, 591–597 (1984)
11 Bolotin, V.V.: Reliability against fatigue fracture in presence of sets of cracks. Engineering Fracture Mechanics **53**, 753–759 (1996)
12 Yang, J.N., Manning, S.D.: A simple second order approximation for stochastic crack growth analysis. Engineering Fracture Mechanics **53**, 677–686 (1996)
13 Lua, Y.J., Liu, W.K., Belytschko, T.: A stochastic damage model for the rupture prediction of a multi-phase solid, Part II: Statistical approach. International Journal of Fracture **55**, 341–361 (1992)
14 Liu, W.K., Chen, Y., Belytschko, T., et al.: Three reliability methods for fatigue crack growth. Engineering Fracture Mechanics **33**, 733–752 (1996)
15 McDowell, D.: An engineering model for propagation of small cracks in fatigue, Engineering Fracture Mechanics **56**, 357–377 (1997)
16 Rybaczuk, M., Stoppel, P.: The fractal growth of fatigue defects in materials. International Journal of Fracture **103**, 71–94 (2000)
17 Lua, Y.J., Liu, W.K., Belytschko, T.: Elastic interactions of a fatigue crack with a micro-defect by the mixed boundary integral equation method. International Journal for Numerical Methods in Engineering **36**, 2743–2759 (1993)
18 Carpineri, A., Monetto, I.: Snap-back analysis of fracture evolution in multi-cracked solids using boundary element method. International Journal of Fracture **98**, 225–241 (1990)
19 Ma, H., Guo, Z., Dhanasekar, M., et al.: Efficient solution of multiple cracks in great numer using eigen COD boundary integral equations with iteration procedure. Engineering Analysis with Boundary Elements **37**, 487–500 (2013)
20 Budyn, E., Zi, G., Moes, N., et al.: A method for multiple crack growth in brittle materials without remeshing. International Journal for Numerical Methods in Engineering **61**, 1741–1770 (2004)
21 Lo, S.H., Dong, C.Y., Cheung, Y.K.: Integral equation approach for 3D multiple-crack problems. Engineering Fracture Mechanics **72**, 1830–1840 (2005)
22 Krysl, P., Belytschko, T.: The element free Galerkin method for dynamic propagation of arbitrary 3-D cracks. Inernational Journal for Numerical methods in Engineering **44**, 767–800 (1999)
23 Rabczuk, T., Bordas, S., Zi, G.: A three-dimensional meshfree method for continuous multiple-crack initiation, propagation and junction in statics and dynamics. Computational mechanics **40**, 473–495 (2007)
24 Miao, Y., He, T.G., Yang, Q., et al.: Multi-domain hybrid boundary node method for evaluating top-down crack in asphalt pavements. Engineering Analysis with Boundary Element **34**, 755–760 (2010)
25 Miao, Y., Wang, Q., Liao, B.H., et al.: A dual hybrid boundary node method for 2D elastodynamics problems. Computer Modeling in Engineering & Science **53**, 1–22 (2009)
26 Miao, Y., He, T.G., Luo, H., et al.: Dual hybrid boundary node method for solving transient dynamic fracture problems. CMES: Computer Modeling in Engineering & Science **85**, 481–498 (2012)
27 Yan, F., Feng, X.T., Pan, P.Z., et al.: A continuous-discontinuous cellular automaton method for regular frictional contact problems. Archive of Applied Mechanics **83**, 1239–1255 (2013)
28 Pan, P.Z., Yan, F., Feng, X.T.: Modeling the cracking process of rocks from continuity to discontinuity using a cellular automaton. Computer & Geosciences **42**, 87–99 (2012)
29 Belytschko, T., Black, T.: Elastic crack growth in finite elements with minimal remeshing. Inernational Journal for Numerical methods in Engineering **45**, 601–620 (1999)
30 Osher, S., Sethian, J.A.: Fronts propagating with curvature-dependent speed: algorithms based on Hamilton-Jacobi formulations. Journal of Computational Physics **79**, 12–49 (1988)
31 Stolarska, M., Chopp, D.L., Moes, N., et al.: Modelling crack growth by level sets in the extended finite element method. Inernational Journal for Numerical Methods in Engineering **51**, 943–960 (2001)
32 Sethian, J.: Evolution, implementation and application of level set and fast marching methods for advancing fronts. Journal of Computational Physics **169**, 503–555 (2001)
33 Rao, Q.H., Sun, Z.Q., Stephansson, O., et al.: Shear fracture (Mode II) of brittle rock. International Journal of Rock and Mining Science **40**, 355–375 (2003)
34 Bobet, A., Einstein, H.H.: Numerical modeling of fracture coalescence in a model rock material. International Journal of Fracture **92,** 221–252 (1998)
35 Li, S.C., Chen, Y.M.: Numerical manifold method for crack tip fields. China Civil Engineering Journal **38**, 96–102 (2005)
36 Wong, R.H.C., Chau, K.T., Tang, C.A., et al.: Analysis of crack coalescence in rock-like materials containing three flaws: Part I. Experimental approach. International Journal of Rock Mechanics and Mining Science **38**, 909– 924 (2001)
37 Zhou, X.P., Yang, H.Q., Dong, J.: Numerical simulation of multiple-crack growth under compressive loads. Chinese Journal of Geotechnical Engineering **32**, 192–197 (2010)
38 Feng, X.T., Ding, W.X., Zhang, D.X.: Multi-crack interaction in limestone subject to stress and flow of chemical solution. International Journal of Rock Mechanics and Mining Science **46**, 159–171 (2009)
39 Pan, P.Z., Ding, W.X., Feng, X.T. et al.: Research on influence of pre-existing crack geometrical and material properties on crack propagation in rocks. Chinese Journal of Rock Mechanics and Engineering **27**, 1882–1889 (2008)